# Structure and Interactions of Fish Type III Antifreeze Protein in Solution

Andrés G. Salvay,[†‡*] Frank Gabel,[§¶‖] Bernard Pucci,[**] Javier Santos,[‡††] Eduardo I. Howard,[†*] and Christine Ebel[§¶‖*]

[†]Instituto de Física de Líquidos y Sistemas Biológicos, Universidad Nacional de La Plata, La Plata, Argentina; [‡]Universidad Nacional de Quilmes, Bernal, Argentina; [§]Commissariat à l'Energie Atomique (CEA), Institut de Biologie Structurale (IBS), Laboratoire de Biophysique Moléculaire, Grenoble, France; [¶]Centre National de la Recherche Scientifique, UMR5075, F-38027 Grenoble, France; [‖]Université Joseph Fourier, Grenoble, France; [**]Laboratoire de Chimie Bioorganique et des Systèmes Moléculaires Vectoriels, Université d'Avignon et des Pays de Vaucluse, Faculté des Sciences, Avignon, France; and [††]Instituto de Química y Físico-Química Biológica, Universidad de Buenos Aires, Buenos Aires, Argentina

ABSTRACT It has been suggested that above a critical protein concentration, fish Type III antifreeze protein (AFP III) self-assembles to form micelle-like structures that may play a key role in antifreeze activity. To understand the complex activity of AFP III, a comprehensive description of its association state and structural organization in solution is necessary. We used analytical ultracentrifugation, analytical size-exclusion chromatography, and dynamic light scattering to characterize the interactions and homogeneity of AFP III in solution. Small-angle neutron scattering was used to determine the low-resolution structure in solution. Our results clearly show that at concentrations up to 20 mg $mL^{-1}$ and at temperatures of 20°C, 6°C, and 4°C, AFP III is monomeric in solution and adopts a structure compatible with that determined by crystallography. Surface tension measurements show a propensity of AFP III to localize at the air/water interface, but this surface activity is not correlated with any aggregation in the bulk. These results support the hypothesis that each AFP III molecule acts independently of the others, and that specific intermolecular interactions between monomers are not required for binding to ice. The lack of attractive interactions between monomers may be functionally important, allowing for more efficient binding and covering of the ice surface.

## INTRODUCTION

Antifreeze proteins (AFPs) are characterized by their ability to bind ice and prevent its growth and recrystallization (1,2). The inhibition of ice growth results in a decrease of the freezing point without changing the melting point by means of a noncolligative mechanism (3,4). The difference between these two temperatures, termed thermal hysteresis, is widely used as an indicator of AFP activity (5). It allows organisms to achieve a supercooled state of body fluids. A two-step adsorption and growth inhibition mechanism for the interaction of AFPs with ice was previously proposed (6). In this model, AFP molecules bind to well-defined sites on the ice surface. Ice may continue to grow through the adsorbed AFP impurities, developing a curved growth front. The increased surface area and curvature make an energetically less favorable configuration and lead to termination of crystal growth, a phenomenon known as the Kelvin effect (2,7,8). Although AFPs have been extensively studied, the detailed interactions by which they inhibit ice growth and recrystallization are not completely understood.

To date, five different groups of polar fish AFPs have been described (Types I–IV and antifreeze glycoproteins) (9,10). Each group contains several isoforms and exhibits a characteristic taxonomic distribution. Our work is centered on fish AFP III, a prototypical globular AFP of 7 kDa present in members of the subclass Zoarcoidei. AFP III has been the subject of a large number of experimental and computational studies (2), as well as biotechnological investigations (11). In addition to its antifreeze activity, AFP III (like some other AFP families) decreases the hypothermic damage in living cells during low-temperature preservation above 0°C, in the absence of ice (12,13). The molecular mechanism behind this protection remains unclear. The structure of AFP III has been described by NMR (14,15) and x-ray crystallography (16,17), and is being studied by neutron diffraction (18). It shows a globular $\beta$-clip fold of dimensions 24 Å × 26 Å × 40 Å, and exhibits a flat ice-binding surface (5,19,20).

Many proteins have a tendency to interact among themselves, achieving in this way their biofunctionality. To understand the complex activities of AFP III (i.e., the inhibition of ice growth and recrystallization at subzero temperatures and the protection of cold-sensitive cells from hypothermic damage at low but above zero temperatures), a comprehensive description of its association state and structural organization in solution is essential.

It has been suggested that cooperative interactions between AFP molecules on the ice surface are required for complete inhibition of ice crystal growth. Wen and Laursen (21) noted that for Type I AFP, which comprises a single $\alpha$-helix of 37 amino acid residues, the relationship between the AFP concentration and the inhibition of ice growth is biphasic. At low concentration, ice grows along both the *c* and *a* axes to produce a crystal with a constant *c*/*a* axis ratio of ~3.3. Above a critical AFP concentration, the ice crystal

*Submitted July 1, 2009, and accepted for publication April 14, 2010.*

*Correspondence: andres@iflysib.unlp.edu.ar or howard@iflysib.unlp.edu.ar or christine.ebel@ibs.fr

Editor: Edward H. Egelman.



0006-3495/10/07/0609/10 $2.00

doi: 10.1016/j.bpj.2010.04.030

stops growing and thermal hysteresis is observed. The authors proposed that AFP binding is reversible at low concentrations because the individual interactions between an AFP molecule and ice are weak (22). At high concentrations, the AFP molecules begin to bind cooperatively through side-by-side interpeptide hydrophobic interactions (22).

A comparable bimodal relationship between the protein concentration and the inhibition of ice growth has been observed in globular AFP III (23). To test the need for cooperativity in AFP III binding, DeLuca and co-workers (24) constructed AFP-fusion proteins with an overall diameter far exceeding that of AFP III to prevent interpeptide interactions. The fusion proteins did not suffer any loss of thermal hysteresis activity and were generally more active than the free AFP. These results are consistent with a model in which AFP molecules bind independently to ice.

In contrast, Du et al. (25–27) suggested that specific interactions between AFP III proteins are required for binding to ice, and that the self-assembly of AFP III on the surface of ice may be expected. Observing that the surface of AFP III presents hydrophilic and hydrophobic regions, and based on ice nucleation, surface tension, and dynamic light scattering (DLS) studies, they proposed that above a critical protein concentration value (2.5 mg/mL), the amphipathic AFP III self-assembles into micelle-like structures; moreover, they suggested that these aggregation properties could play a key role in antifreeze activity (25–27).

We recently studied the electro-optical properties of AFP III in solution (28). We found that the concentration dependence of the electrical properties exhibited nonideal behavior. These results could conceivably support the protein aggregation hypothesis, but may also be explained by the existence of some other types of intermolecular interactions. In the work presented here, our goal was to directly investigate the association state, interactions, and solution structure of AFP III. Such information is a prerequisite for understanding the activity of AFP III and clarifying whether AFP III molecules act independently or specific interactions between monomers are required for cooperative binding to ice.

We used analytical ultracentrifugation (AUC), which combines particle separation and analysis into a powerful technique for characterizing sample homogeneity and rigorously determining the protein size, mass, and interactions (29). Analytical size-exclusion chromatography (SEC) coupled to multi-angle laser light scattering (MALLS), and DLS were also applied to confirm the AUC results in the absence of a centrifugal field. Small-angle neutron scattering (SANS), a key technique for determining the low-resolution structure of macromolecules in solution (30), was used to compare the known crystallographic structure with the structure in solution. The surface activity properties of AFP III at the air/water interface were also studied.

Our results clearly show that AFP III at concentrations up to 20 mg $mL^{-1}$ is monomeric in solution, at 20°C, 6°C, and 4°C, and adopts a structure compatible with the crystallographic structure. Surface tension measurements show a propensity of AFP III to localize at the air/water interface, but this surface activity is not correlated with any aggregation of the protein in the bulk. These data are essential for elucidating how AFP III functions.

## MATERIALS AND METHODS

The HPLC-12 isoform from ocean pout (*Macrozoarces americanus*) AFP III, corresponding to the protein sequence code P19614 and the 1HG7 PDB high-resolution structure (20), was overexpressed in *Escherichia coli* as inclusion bodies, solubilized in 2 M urea, and purified as described previously (28). The purified protein was dialyzed twice against distilled and deionized water and lyophilized. Solutions of AFP III at different concentrations were prepared by dissolution of the same lyophilized protein batch in $H_2O$ and $D_2O$, or in 150 mM NaCl, 20 mM Tris-HCl buffer at pH 7.5 (Solvent A). We chose to use pure and deionized water (either $H_2O$ and $D_2O$) because other studies on the same protein were performed under identical conditions (25–27). The chemical purity of the sample was checked by Tris/tricine sodium dodecyl sulfate polyacrylamide gel electrophoresis and mass spectrometry with a molecular mass of 7034 Da (see Fig. S1 in the Supporting Material). The molar extinction coefficient at 280 nm was experimentally obtained as 1568 ± 33 $M^{-1}cm^{-1}$ ($E_{0.1\%}$ = 0.223 ± 0.005 mg $mL^{-1}cm^{-1}$; see Supporting Material). To check the proper folding of our protein in pure $H_2O$, we measured the far and near ultraviolet circular dichroism (CD) spectra between 180 and 260 nm, and 250 and 340 nm, respectively (Fig. S2). The spectra resembled those obtained for AFP III in different solvents (28). Additionally, this lyophilized protein batch was successfully used in crystallization experiments. AFP III was shown to be stable in $H_2O$ and $D_2O$ at 4°C, 6°C, and 20°C (28). The partial specific volume $\bar{v}$ of AFP III is required for the interpretation of SANS and/or AUC experiments, and $\bar{v}$ = 0.758 ± 0.005 mL $g^{-1}$ was determined from precise density measurements (see Fig. S3). The experimental values of molar mass, molar extinction coefficient at 280 nm, and $\bar{v}$ are very close to those obtained from the amino acid content.

### Experimental methods

Sedimentation velocity (SV) experiments were performed at 20°C in $H_2O$ and $D_2O$, and at 4°C in Solvent A for AFP III samples at concentrations typically between 0.5 and 20 mg $mL^{-1}$. Sedimentation equilibrium (SE) experiments were performed at 4°C in Solvent A for AFP III samples between 0.5 and 10 mg $mL^{-1}$. The sedimentation depends on the sedimentation and diffusion coefficients, $s$ and $D$, of the macromolecules in solution and their interactions; $s$ and $D$ are related to the macromolecular molar mass, $M$, which can also be obtained directly from the SE. The Supporting Material gives details on the SV and SE experiments, all programs used for the analysis, the theoretical background, and principles of the analysis.

Analytical SEC combined with MALLS, DLS, and surface tension experiments are also described in the Supporting Material.

SANS experiments were carried out at 6°C on the D22 small-angle diffractometer at the Institut Laue-Langevin (Grenoble, France). See the Supporting Material for details regarding the experiments, analysis, and programs used for the analysis.

## RESULTS

### Sedimentation velocity of AFP III: general behavior

The homogeneity of the molecular mass and size of AFP III in solution between 0.5 and 20 mg $mL^{-1}$ was measured using AUC SV. Experiments were done in Solvent A at 4°C, as

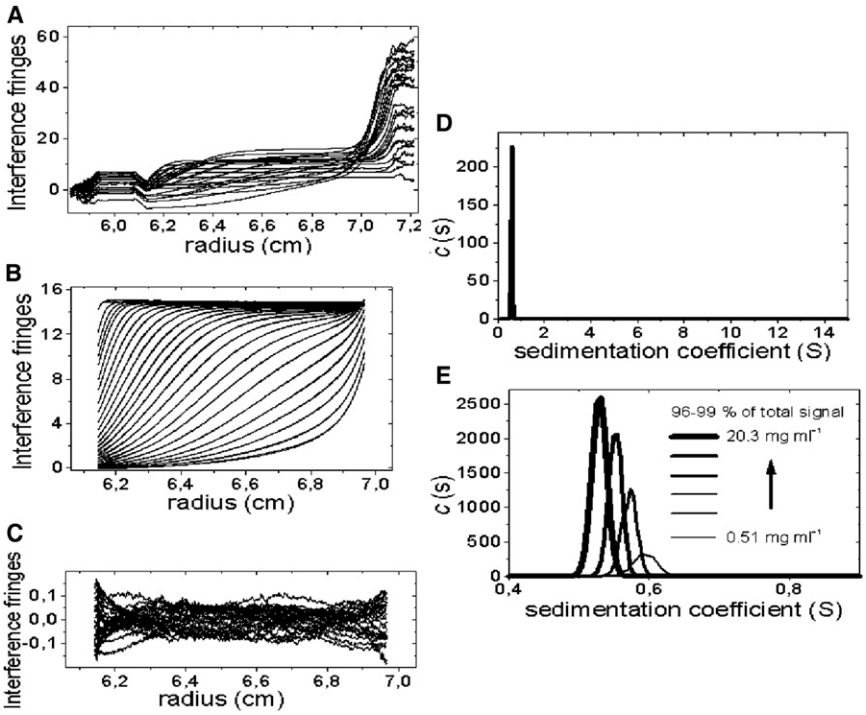


FIGURE 1 SV of AFP III at 60,000 rpm and 4°C in 20 mM Tris-HCl, 150 mM NaCl, pH 7.5. (*A*) Selection of raw data for AFP III at 5.1 mg $mL^{-1}$. (*B*) Superposition of experimental (*dots*) and fitted (*continuous line*) profiles corrected for all systematic noise for AFP III at 5.1 mg $mL^{-1}$. The last profiles correspond to 20 h of sedimentation. The fit was obtained from the $c(s)$ analysis with the program SEDFIT. (*C*) Superposition of the differences between the experimental and fitted curves. (*D*) Corresponding $c(s)$ distribution in the range of 0.1–15 S. (*E*) Superposition of the $c(s)$ distributions for different concentrations of AFP III in the range of 0.4–0.9 S, corresponding to >96% of the total signal. The concentrations are 0.51, 1.0, 5.1, 10.2, 15.2, and 20.3 mg $mL^{-1}$. For clarity, the interference signal is multiplied by a factor of 4 for the experiments performed in 0.3 cm optical path centerpieces, for concentrations higher than 10 mg $mL^{-1}$. Concentrations 0.51 and 1.0 mg $mL^{-1}$ are not visible in the figure because of the low signal in comparison with the high concentrations.

well as in $H_2O$ and $D_2O$ at 20°C, in view of the SANS experiments. Sedimentation of AFP III displays a well-defined boundary in Solvent A (Fig. 1), as well as in $D_2O$ (profiles not shown) and in $H_2O$ (Fig. S4). AFP III sediments more slowly in $D_2O$ than in $H_2O$, and at 4°C compared to 20°C, which is expected because of the larger density (in $D_2O$) and viscosity (in $D_2O$ or at 4°C) of the solvent.

## Enhanced van Holde-Weischet analysis of the SV of AFP III

We used the van Holde-Weischet analysis (31) for a qualitative evaluation of heterogeneity and interaction. Fig. S5 compares the van Holde-Weischet plots obtained for AFP III between 5 and 20 mg $mL^{-1}$ at 42,000 rpm and 20°C in $H_2O$, and at 60,000 rpm and 4°C in Solvent A. For all concentrations and experimental conditions, the extrapolations to infinite time (intercepts) show one well-defined group of $s_{20,w}$ values around 1 S, indicating the absence of aggregates. The large diffusion of AFP III limits the scope of the analysis and at least partly explains the limited scattering of the intercepts at 42,000 rpm compared to 60,000 rpm. At 60,000 rpm, it is clear that increasing the AFP III concentration makes the extrapolated values of $s_{20,w}$ decrease from slightly above to slightly below 1 S, indicating nonideality. In addition, the convergence of the lines is shifted to the right with increasing concentration, which is further evidence of the expected nonideality effects. The origin of the asymmetry of the plot close to the intercept is not clear. Clearly, however, AFP III samples appear homogeneous with no evidence of association equilibrium.

## Size distribution analysis of the SV of AFP III

Sedimentation profiles were then analyzed in terms of a distribution of ideal particles using the $c(s)$ analysis (32). The $c(s)$ method deconvolutes the effects of diffusion broadening, which results in high-resolution sedimentation coefficient distributions. The superposition of the experimental and modeled sedimentation profiles for AFP III in Solvent A at 5.1 mg $mL^{-1}$ are shown in Fig. 1 *B*. The residuals are only imperfectly randomly distributed around zero (Fig. 1 *C*), which is reasonably related to the nonideality of the concentrated solutions. However, the maximum residual is <1% of the total number of interference fringes (here, 0.1/17 fringes) for all tested concentrations, which is not bad. The $c(s)$ analysis in the range of 0.1–15 S shows one major, well-defined peak (96% of the total signal) at 0.59 S (Fig. 1 *D*). Fig. 1 *E* shows the superposition of $c(s)$ curves, built in the range of 0.5–0.9 S, for AFP III in Solvent A and 4°C at different concentrations between 0.51 and 20.3 mg $mL^{-1}$. For all of the samples, a single contribution representing 96–99% of the total signal is observed at ≈0.6 S. The *s*-value slightly decreases with increasing protein concentration, indicating nonideality. Experiments performed in $D_2O$ and $H_2O$ at 20°C, at protein concentrations in the same range, similarly show only one main species—at ≈0.5 S and 1.0 S, respectively—corresponding to 98–99% and 97–99%, respectively, of the total signal (data not shown and Fig. S4, respectively). Thus, the AFP III samples are essentially homogeneous and there is no evidence of concentration-dependent association or aggregation.

## Noninteracting species model analysis of the SV of AFP III and nonideal sedimentation

The SV profiles of AFP III were analyzed in terms of independent noninteracting species. The relevance of large species attributed to aggregates is negligible because when the data are analyzed in terms of two species (monomer and aggregates), the program converges for all concentrations to the model of a single species. The species is characterized by a number of interference fringes, $J$, proportional to concentration; a sedimentation coefficient, $s$; and an apparent diffusion coefficient, $D_{app}$. $J$ and $s$ from the $c(s)$ analysis are (within experimental error) those of the noninteracting species model. We note that $J$ for AFP III in $H_2O$, $D_2O$, and Solvent A is perfectly linearly related to the total concentration $c$ (see Fig. S6). The slope of the linear regression gives the value of the refractive index increment $\partial n/\partial c = 0.189 \pm 0.003$ mL g$^{-1}$, which agrees with the standard value of 0.186 mL g$^{-1}$ tabulated for soluble and globular proteins. This indicates that the estimate of $J$ is precise, and the total protein concentration and the concentration of the single species of AFP III are equivalent, confirming that aggregates, if they exist, can only be present in negligible amounts. Linear regressions of $s^{-1}(c)$ and $D_{app}(c)$ are shown in Fig. S7 and results are reported in Table 1. The slight decrease of the $s$-values under all solvent conditions with increasing AFP III concentration is related to nonideality effects. The concentration-dependency factor $k_s$ is positive, which corresponds to weak repulsive interparticle interactions related to excluded volume effects (see the Supporting Material). If there were weak interactions leading to self-association, then upon increasing $c$, $s$ would increase from the sedimentation coefficient at infinite dilution, $s_0$, and the related $k_s$ would be negative. The shape of the sedimentation boundary is affected by the macromolecular diffusion, which may change with concentration, as well as by the concentration dependency of $s$ (33). This means that $D_{app}$ (calculated from an inappropriate model of a noninteracting species) is not a diffusion coefficient except in the ideal case, i.e., at infinite dilution. The intercept in Fig. S7 indeed represents the diffusion coefficient at infinite dilution, $D_0$.

## Molecular characteristics of AFP III in solution from the SV

The hydrodynamic radius $R_S$ and the molecular weight $M$ of AFP III in $H_2O$ and $D_2O$ at 20°C, and in Solvent A at 4°C, are derived from the extrapolated values to infinite dilution $s_0$ and $D_0$ (see Supporting Material) and given in Table 1. The experimental value of $M$ is in excellent agreement with that calculated for monomeric AFP III from the amino acid sequence or measured by mass spectrometry. The experimental value of $R_S = 1.6$ nm agrees with the hydrodynamic radius of monomeric AFP III calculated from the 1HG7 PDB entry and using the program HYDROPRO (34). It corresponds to a frictional ratio of 1.25, which is a usual value for a compact protein. A value of 1.17 is calculated from tabulated data for a 7 kDa native folded protein (35,36). Thus, AFP III is a monomer of AFP III under all of the experimental conditions.

## Sedimentation equilibrium experiments

SE experiments are a rigorous way to ascertain the molar mass of a macromolecule in solution. Experiments were done at 4°C in Solvent A at concentrations of 0.5, 1, 2.5, 5.1, and 10.2 mL$^{-1}$, and at three angular velocities. Fitting each sample separately gives molar masses decreasing from 7.8 kDa for the lowest concentration to 6.3 kDa for the largest one (not shown). The decrease of these values may be related to nonideality (see Supporting Material). However, as can be seen in Fig. 2, the simplest model of one ideal species allows all the data to be nicely fitted. It provides a molar mass of 7 kDa corresponding to AFP III as a monomer.

## Analytical SEC with light-scattering detection

We also performed SEC experiments combined with refractometry and multi-angle light scattering (Fig. S8), which allowed us to evaluate the sample homogeneity and determine, in an absolute way, the molar mass of macromolecules and assemblies in solution (37). The sample eluted from the SEC column at 20°C for AFP III in Solvent A as a single peak. The single, well-defined elution peak confirms the nonexistence of aggregates of AFP III in solution, since light-scattering detection emphasizes the detection of the largest species. The absolute molecular mass of the species corresponding to the peak was determined at each point of the chromatogram. The polydispersity factor is equal to $1.04 \pm 0.07$, suggesting a monodisperse sample, whereas $M$ is 7.3 kDa, which is in excellent agreement with the molecular mass obtained from SV experiments and further demonstrates that AFP III is a monomer in solution.

**TABLE 1 Concentration-dependence analysis of sedimentation of AFP III in $H_2O$ and $D_2O$ at 42,000 rpm and 20°C, and in 20 mM Tris-HCl, 150 mM NaCl, pH 7.5 (Solvent A), at 60,000 rpm and 4°C**

| | $s_0$ (S) | $s_{0,20,w}$ (S) | $k_s$ (mL g$^{-1}$) | $D_0$ ($10^{-7}$cm$^2$ s$^{-1}$) | $D_{0,20,w}$ ($10^{-7}$cm$^2$ s$^{-1}$) | $M$ (kDa) | $R_S$ (nm) |
|---|---|---|---|---|---|---|---|
| $H_2O$ | 1.00 ± 0.01 | 1.00 ± 0.01 | 5.9 ± 0.3 | 13.7 ± 0.1 | 13.7 ± 0.1 | 7.3 ± 0.2 | 1.6 ± 0.1 |
| $D_2O$ | 0.59 ± 0.01 | 1.09 ± 0.02 | 5.8 ± 0.3 | 11.0 ± 0.1 | 13.6 ± 0.2 | 8.0 ± 0.2 | 1.6 ± 0.1 |
| Solvent A | 0.63 ± 0.02 | 1.03 ± 0.03 | 8.8 ± 0.7 | 8.0 ± 0.2 | 13.5 ± 0.3 | 7.7 ± 0.4 | 1.6 ± 0.1 |

Errors are estimated from the linear regression analysis of data of Fig. S7 and propagated according to the rules of errors.

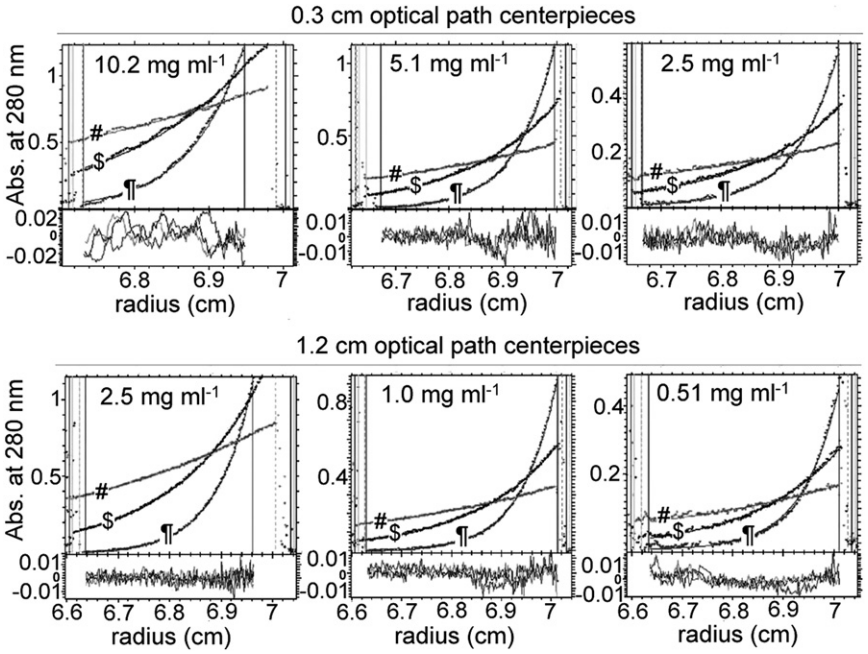


FIGURE 2 Equilibrium sedimentation profiles of AFPIII at 4°C in Solvent A. Each panel shows the superposition of the experimental equilibrium profiles (*dot*) and their fit (*line*) (*upper part*) obtained at 20,000 rpm (#), 32,000 rpm ($), and 50,000 rpm (¶), and the superposition of the differences between the experimental and fitted curves (*lower part*). All data were globally fitted using the program Sedphat in the model of one noninteracting species without noise evaluation, but adjusting a baseline for each cell (−0.017, −0.0143, −0.002, −0.008, −0.011, and −0.021 from *top left* to *bottom right panels*). This very simple and constrained model provides a rather good superimposition of the fitted and experimental profiles. Data were considered up to $A_{280} = 1.2$, i.e., to a maximum concentration of 17 mg $mL^{-1}$. The determined molecular mass is 6966 Da.

## DLS measurements

The dependence of the size and polydispersity of AFP III with the concentration was also investigated by means of DLS. DLS experiments at 20°C were performed for five concentrations of AFP III ranging from 0.55 to 22.1 mg $mL^{-1}$ in $H_2O$. The autocorrelation functions were described well by a single-exponential decay for all concentrations, with typical baseline values of 1.001–1.002, which corresponds to a monomodal or primarily monomodal distribution without polydispersity. At 22.1 and 11.0 mg $mL^{-1}$, DLS analysis revealed a 100% homogeneous sample. At the smallest concentrations of 5.5, 2.8, and 0.55 mg $mL^{-1}$, small additional contributions were detected at 51, 55, and 160 nm, respectively, which were clearly related to dust and did not have to be considered. The value of $R_S$ obtained for AFP III was $\approx$1.4 nm and did not vary significantly with AFP III concentration in the range of 0.55–22.1 mg $mL^{-1}$ (see Table S1). Again, there is no indication of any association of the protein. The $R_S$ values obtained from DLS are in reasonable agreement with what was experimentally determined by SV or calculated from the crystallographic structure.

## AFP III structure in solution: SANS experiments

Fig. 3 *A* shows the experimental scattering curves (normalized to the highest concentration and scaled to one) for AFP at the three concentrations measured at 6°C, as well as the theoretical curve calculated from PDB entry 1HG7. In the concentration range explored, the experimental scattering curves agree excellently with the theoretical curve over the entire angular range. From our data, there is no evidence of any higher oligomeric states. The experimental radii of gyration (Fig. 3 *B*)—10.40 ± 0.03, 10.33 ± 0.03, and 10.28 ± 0.03 Å (AFP III at 21.6, 16.2, and 10.8 mg $mL^{-1}$)—are equally in excellent agreement with that from the PDB structure (10.2 Å). Minor differences may be due to effects of hydration shell water (38). We therefore conclude that AFP III is in a monomeric state in solution, and there are no structural differences between the crystal structure and the structure in solution. This is further corroborated by a comparison of the back-calculated scattering curve from an artificial AFP III dimer with the experimental data, which are significantly different (Fig. S9).

In addition, we calculated a pair distance distribution function $p(r)$ from the experimental data and the monomeric 1HG7 (Fig. S10). Both display a slightly asymmetric Gaussian shape indicative of a compact particle deviating slightly from a sphere. The minor deviations at larger distances may be due to disordered side chains on the surface of the protein. Fig. 3 *C* shows the superposition of the DAMMIN-created low-resolution shape and 1HG7. They are very similar, as reflected by a low normalized spatial discrepancy criterion of 0.74 (values $< 1.0$ indicate similarity; the smaller the value, the more similar are the two structures).

## Surface-active properties of AFP III at the air/water interface

The relative surface activity of AFP III was determined from measurements of surface tension as a function of protein concentration in $H_2O$ at 20°C. As we can see in Fig. 4, AFP III induces a low decrease of surface tension when the protein concentration increases. For the first experiment (stirring time of 5 min), there is possibly a plateau between 2.3 and 3.7 mg $mL^{-1}$, and above an estimated value of 3.7 mg $mL^{-1}$, a break in the curve is observed and the surface

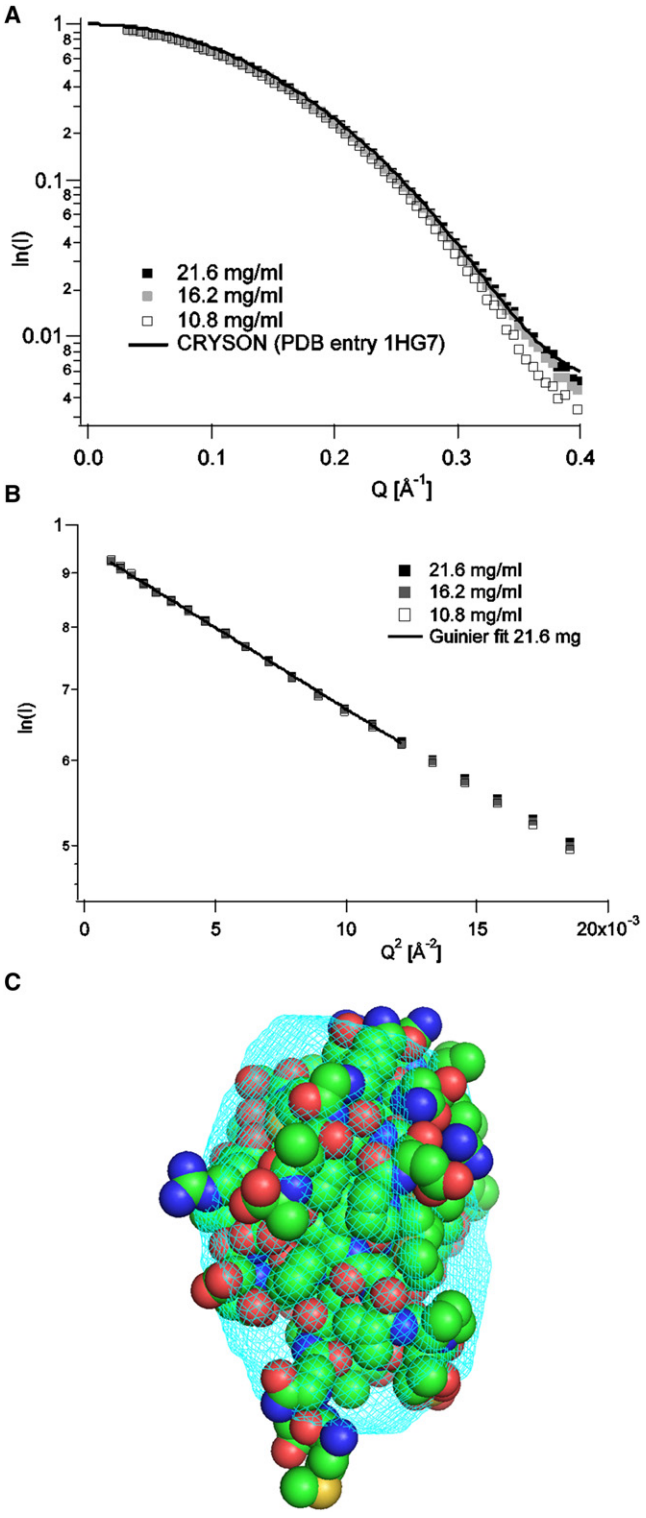


FIGURE 3 SANS of AFPIII at 6°C. (*A*) Experimental neutron scattering curves from AFP in $D_2O$ at three concentrations and normalized to the highest concentration and scaled to one, as well as the theoretical one from PDB entry 1HG7 (calculated with CRYSON). (*B*) Guinier plots of the same experimental data. (*C*) Superposition of low-resolution structure from experimental data and high-resolution PDB 1HG7 using the program SUPCOMB. The figure was created using the program PYMOL (http://www.pymol.org).

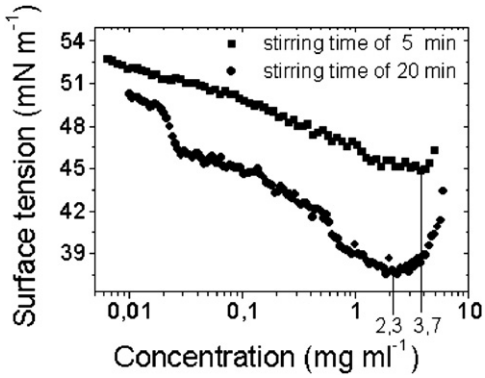


FIGURE 4 Surface tension of AFP III in $H_2O$ at 20°C as a function of concentration. An initial concentration of 4.8 (■) and 6 (●) mg mL$^{-1}$ was successively diluted with a stirring time of 5 (■) and 20 (●) min between each dilution and measurement.

tension increases with increasing AFP III concentration up to 4.8 mg mL$^{-1}$. However, the evidence for these features in Fig. 4 seems rather poor, and they could just be noise. For this reason, we performed a second experiment from a stock solution at 6 mg mL$^{-1}$, with a longer time between each measurement. Under these conditions, we observe a minimum value of the surface tension at 2.3 mg mL$^{-1}$, which is comparable to that measured at 25°C by Du et al. (25). This minimum point should indicate a rearrangement of the AFP III on the air/water interface (see below). The discrepancy between our two curves is attributed to slow processes at the interface reaching equilibrium. We note a feature common to the two experiments: the value of the surface tension at the lowest measured concentration (0.006 or 0.01 mg mL$^{-1}$) is ~20 mN m$^{-1}$ below the value of pure water.

## DISCUSSION

Our aim in this work was to characterize the interactions of AFPIII in solution and the structure of the association states, if any. In the context of a structural study, the purity and quality of the purified recombinant protein sample used here were checked by means of chemical studies, density measurements, and optical spectroscopy. The experimental values of the molar extinction coefficient, partial specific volume, and polypeptide molar mass coincide with those predicted from the amino acid sequence of AFP III. Also, the CD spectra were the same as those described in the literature (28). AFP III was studied in a large range of protein concentrations, with the largest being close to the physiological concentration (the ocean pout, *M. americanus*, produces type III AFPs at a level of ~25 mg mL$^{-1}$ in serum during winter (20)).

### AFP III is a monomer at up to 20 mg mL$^{-1}$

We used different but complementary experimental methodologies for our purpose. AUC was used to investigate the hydrodynamic behavior of AFP III. Analysis of SV

experiments using numerical solutions of the Lamm equation can adequately describe the homogeneity and hydrodynamic behavior of complex biomolecules in solutions (39–41). Our SV experiments clearly show that, under all of our experimental conditions (in $H_2O$, $D_2O$, or Solvent A, at 4°C and 20°C), AFP III was highly homogeneous in a large range of concentrations (from 0.5 up to 22 mg $mL^{-1}$). The same behavior was observed in His-tagged AFP III (results not shown). The molecular mass ($M$ = 7.3 kDa) and hydrodynamic radius ($R_S$ = 1.6 nm) of the single species sedimenting in the SV experiments are very close to those predicted from the amino acid sequence and the crystallographic structure of an AFP III monomer, which shows a compact structure with half dimensions of 1.2 nm × 1.3 nm × 2.0 nm (16,17). The concentration dependence of the sedimentation coefficient is the opposite of what would be expected if there were interactions leading to association between monomers, and can be simply related to repulsive excluded volume effects (see Supporting Material). Complementary SE, performed at 4°C and in Solvent A for samples between 0.5 and 10 mg $mL^{-1}$, and analytical SEC performed at 20°C and in Solvent A confirmed the homogeneity and monomer state of AFP III. Liu and Du (26) reported two sizes of molecules from DLS measurements of AFP III in pure $H_2O$ at concentrations of 0.5 and 2.5 mg $mL^{-1}$. The smallest, with $R_S$ = 0.55 nm, which the authors associated with monomeric protein, was present at the two AFP III concentrations, whereas the largest, with $R_S$ = 1.4 nm, which they related to AFP III aggregates, was observed only at 2.5 mg $mL^{-1}$ and dominated the signal. Based on the structures reported for this protein (14–20), it is not reasonable to propose a hydrodynamic diameter of 1.1 nm for a monomeric state. We reproduced the DLS experiments with AFP III between 0.5 and 22.1 mg $mL^{-1}$ under the same experimental conditions. The AFP III solutions were homogeneous (with minor amounts of very large particles interpreted as dust at the lowest concentrations) with particles of $R_S$ ~ 1.3 nm corresponding to the protein monomer. Thus, in the light of our results, the largest particle observed by Liu and Du corresponds to the monomer of type III AFP, and the smallest ($R_S$ ~ 0.5 nm) may be a solvent component or artifact. It is extremely difficult to perform DLS experiments on diluted samples, and small-angle scattering is very sensitive to large particles. The SANS experiments provided no evidence for associated states of AFP III in solution, and confirmed the presence of AFP III as a monomer in the 10–20 mg $mL^{-1}$ range. Furthermore, the SANS scattering curves superimposed with that calculated from the AFP III crystal structure emphasize that the solution structure is at least grossly similar to that described from crystallography. The SANS experiments were done at 6°C in $D_2O$, which confirms that AFP III does not auto-associate at a temperature close to freezing (the melting point of $D_2O$ is 3.82°C).

## Does the studied recombinant protein behave similarly to the native AFP III from fish plasma?

The ocean pout, *M. americanus*, produces a mixture of at least 12 type III AFPs isoforms (42,43). Among these, the HPLC-12 isoform studied here has been the most extensively studied and was the first to have its three-dimensional structure solved (14). In earlier structural studies (14,16,44), the HPLC-12 component (and also other isoforms) was produced by recombinant methods (45), and in the last 15 years the recombinant protein has been used in all kinds of experiments because no difference has been found between the natural and recombinant HPLC-12 isoforms. There is no consensus sequence for phosphorylation or glycosylation, and, as far as we know, no evidence of a possible posttranslational modification has been published. From *E. coli*, the isoform HPLC-12 is obtained in inclusion bodies, which are usually dissolved in urea 6 M or 8 M (46). For the solubilization step, we used only 2 M of urea, which is enough to solubilize the protein but not enough to perturb the native structure (47). A pH value of 4 (used in the standard purification protocol, independently of the source of the protein) does not modify the protein properties, since AFP III is active from pH 2 to pH 11 (46). The crystal structure was solved at pH 4.0–4.5 (18,20,44), and indeed we were able to obtain crystals from our preparation. The monomeric state we observed here is also in agreement with the pioneer studies that characterized AFP III (42,43). The first purification step was at size-exclusion column Sephadex G-75, which has a fractionation range for globular proteins of 3000–80,000 Da. (In their study, Hew et al. (42) reported that ''the chromatography of the ocean pout's serum produced only one peak of macromolecular 'antifreeze' activity having an apparent molecular weight of 10000''.)

## Does the surface tension of AFP III differ from other globular proteins?

Our study was motivated by publications describing the formation of micelle-like structures for AFP III above 2.5 mg $mL^{-1}$, as determined by surface tension measurements (25,27). Because we do not observe such assemblies in solution, we chose to reinvestigate the behavior of AFP III at the air/water interface. Although our first measurements for AFP III only poorly reproduced the published results (Fig. 4, stirring time of 5 min), our second measurements with a longer equilibration time produced results more similar to those of Du et al. (25), i.e., a minimum value without plateau followed by an increase of surface tension when AFP III concentration exceeded 2.3 mg $mL^{-1}$ (Fig. 4, stirring time of 20 min). A break and a plateau would be expected if the interface were saturated, which happens at the critical micellar concentration for a surfactant. Proteins are naturally amphiphilic, with a primary structure containing both hydrophobic and hydrophilic amino acid residues.

For proteins denatured in foam, an apparent critical micellar concentration can be defined that represents the concentration at which there is complete monolayer coverage at the interface (48). A plateau is also observed for proteins that form structures similar to micelles in solution, such as $\beta$-casein (49,50). It was previously hypothesized that AFP III forms micelles (25), but we have demonstrated that in solution it is monomeric and does not form aggregates up to 20 mg $mL^{-1}$. Therefore, the surface activity of AFP III is not correlated with any aggregation of the protein in the bulk. Does the surface tension of AFP III differ from that of other globular proteins? A common feature in the few globular proteins that have been documented to show changes in the surface tension with concentration is a maximum decrease of ~20 mN $m^{-1}$. This value has been described as being practically independent of the type of protein (the tested proteins had molecular masses between 15 and 150 kDa, whereas that of AFP III is 7 kDa) and the experimental conditions used, with a plateau at low and/or high concentrations. The former is tentatively explained by the formation of a close-packed adsorption protein layer immersed in the aqueous subphase, and the latter by the formation of an ordered, quasi-crystal protein monolayer at the interface (51,52). In our experiments (dilution series), as well as in previous experiments with increasing protein concentrations, AFP III displayed a surface tension that did not exceed 53 mN $m^{-1}$, even at the lowest concentration (0.005 mg $mL^{-1}$). This suggests a propensity of AFP III to be localized at the air/water interface, and we can hypothesize that the variation with concentration of the surface tension would reflect slight modifications in the packing of AFP III at the interface.

Previously published surface tension and DLS experiments, which were not correctly interpreted (as we demonstrate here), led to the proposal that above a critical protein concentration of 2.5 mg $mL^{-1}$, the amphipathic proteins self-assemble to form micelle-like structures with a hydrophobic core and a hydrophilic surface, and suggested that specific protein-protein interactions are required for cooperative binding to ice (25–27). A self-assembly of AFP III on the surface of ice, in a manner similar to that of emulsions of oil in water with amphiphilic surfactants, was proposed (25–27). We have demonstrated that no association of AFP III monomers occurs in the bulk. This suggests that each AFP III molecule acts independently of the others, and that specific intermolecular interactions between monomers may not be required before binding to ice occurs. Our surface tension data, however, confirm the capacity of AFP III to colocalize at the interface. Because of the influence on the dipole moment of the macromolecule, protein surface activity depends on details of the secondary structure (51), and we can speculate that the unusual surface tension behavior of AFP III may be related to its unusual structure, as suggested by CD and Raman optical activity (53), and/or to particular rearrangements of the protein at the surface. Indeed, AFP III has been shown to be flexible (a two-domain tandem structure, with two connected domains tumbling and moving independently, was reported by NMR (54)). The low value of the surface tension at low protein concentration may be important for the efficiency of the protein functionality observed at low concentrations (55).

## CONCLUSIONS

Currently, there is no general theory that can explain all the activities of the so-called ''antifreeze'' proteins, i.e., inhibition of ice growth at millimolar concentrations, inhibition of ice recrystallization at nanomolar concentrations, and decreased damage during low-temperature preservation of living cells at above-zero temperatures (2,13). These phenomena are observed at different concentrations and temperatures. However, these diverse and complex activities have the same starting point: the protein in aqueous solution. We confirm herein that AFP III is monomeric under a large range of experimental conditions. Our results agree with those obtained by DeLuca and co-workers (24), and support the hypothesis that each AFP III molecule acts independently and that specific intermolecular interactions between monomers are not required for binding to ice. According to the two-step adsorption and growth inhibition mechanism proposed for AFP activity, the complete covering of ice by AFPs is not required for antifreeze activity (6). The nonexistence of attractive interactions between AFP III monomers, as demonstrated here, may be functionally important for more efficient binding and covering of the ice surface. This effect may also be linked to the efficiency of the protein functionality observed at low concentrations (55).

## SUPPORTING MATERIAL

Complementary information on chemical homogeneity of AFP III by gel electrophoresis and mass spectrometry, ultraviolet spectroscopy, extinction coefficient and circular dichroism of AFP III, determination of the partial specific volume of AFP III, analytical ultracentrifugation (AUC), analytical size-exclusion chromatography with light scattering detection, dynamic light scattering, small-angle neutron scattering, and surface tension measurements is available at http://www.biophysj.org/biophysj/supplemental/S0006-3495(10)00528-X.

The authors thank Anne-Sylvie Fabiano and Maher Abla (Avignon) for performing a set of surface tension experiments; Marc Jamin (European Molecular Biology Laboratory, Grenoble Outstation, Unit of Virus Host Cell Interactions) for performing the SEC/MALLS experiments and analysis; Bernard Dublet for performing mass spectrometry measurements; and Isabelle Petit-Hartlein, Antoine Maillard (IBS), B. Raynal (Institut Pasteur Paris), and Thierry Azoulay (Wyatt) for advice. We also thank members of the D22 BAG system for providing SANS beam time at Institut Laue-Langevin; Joe Zaccaï for assistance during the experiments, Alberto Podjarny and Alexandra Cousido (Institut de Génétique et de Biologie Moléculaire et Cellulaire Strasbourg) for help and support in protein production; and Carlo Petosa (IBS) for a critical reading of the manuscript. The SEC/MALLS and mass spectroscopy experiments were done using the SEC/MALLS and mass spectrometry platforms of the Partnership for Structural Biology (PSB) and Institut de Biologie Structurale Grenoble (IBS).

The work was supported by CEA, Centre National de la Recherche Scientifique, Université Joseph Fourier, Universidad de La Plata, and CONICET (PIP 112-200801-03247).

## REFERENCES


1. Davies, P. L., J. Baardsnes, …, V. K. Walker. 2002. Structure and function of antifreeze proteins. *Philos. Trans. R. Soc. Lond. B Biol. Sci.* 357:927–935.
2. Venketesh, S., and C. Dayananda. 2008. Properties, potentials, and prospects of antifreeze proteins. *Crit. Rev. Biotechnol.* 28:57–82.
3. Raymond, J. A., and A. L. DeVries. 1977. Adsorption inhibition as a mechanism of freezing resistance in polar fishes. *Proc. Natl. Acad. Sci. USA.* 74:2589–2593.
4. Davies, P. L., and C. L. Hew. 1990. Biochemistry of fish antifreeze proteins. *FASEB J.* 4:2460–2468.
5. Chen, G., and Z. Jia. 1999. Ice-binding surface of fish type III antifreeze. *Biophys. J.* 77:1602–1608.
6. Wen, D., and R. A. Laursen. 1993. A D-antifreeze polypeptide displays the same activity as its natural L-enantiomer. *FEBS Lett.* 317:31–34.
7. Davies, P. L., and B. D. Sykes. 1997. Antifreeze proteins. *Curr. Opin. Struct. Biol.* 7:828–834.
8. Zachariassen, K. E., and E. Kristiansen. 2000. Ice nucleation and antinucleation in nature. *Cryobiology.* 41:257–279.
9. Ewart, K. V., B. Rubinsky, and G. L. Fletcher. 1992. Structural and functional similarity between fish antifreeze proteins and calcium-dependent lectins. *Biochem. Biophys. Res. Commun.* 185:335–340.
10. Brown, D. J., and F. D. Sonnichsen. 2002. The structure of fish antifreeze proteins. *In* Fish Antifreeze Proteins. K. V. Ewart and C. L. Hew, editors. World Scientific, London. 109–138.
11. Fletcher, G. L., S. V. Goddard, and Y. L. Wu. 1999. Antifreeze proteins and their genes: from basic research to business opportunity. *Chemtech.* 29:17–28.
12. Prathalingam, N. S., W. V. Holt, …, P. F. Watson. 2006. Impact of antifreeze proteins and antifreeze glycoproteins on bovine sperm during freeze-thaw. *Theriogenology.* 66:1894–1900.
13. Hirano, Y., Y. Nishimiya, …, S. Tsuda. 2008. Hypothermic preservation effect on mammalian cells of type III antifreeze proteins from notched-fin eelpout. *Cryobiology.* 57:46–51.
14. Sönnichsen, F. D., B. D. Sykes, …, P. L. Davies. 1993. The nonhelical structure of antifreeze protein type III. *Science.* 259:1154–1157.
15. Miura, K., S. Ohgiya, …, S. Tsuda. 2001. NMR analysis of type III antifreeze protein intramolecular dimer. Structural basis for enhanced activity. *J. Biol. Chem.* 276:1304–1310.
16. Jia, Z., C. I. DeLuca, …, P. L. Davies. 1996. Structural basis for the binding of a globular antifreeze protein to ice. *Nature.* 384:285–288.
17. Ko, T. P., H. Robinson, …, A. H. Wang. 2003. The refined crystal structure of an eel pout type III antifreeze protein RD1 at 0.62-A resolution reveals structural microheterogeneity of protein and solvation. *Biophys. J.* 84:1228–1237.
18. Petit-Haertlein, I., M. P. Blakeley, …, A. Podjarny. 2009. Perdeuteration, purification, crystallization and preliminary neutron diffraction of an ocean pout Type III anti-freeze protein. *Acta Crystallogr. Sect. F Struct. Biol. Cryst. Commun.* 65:406–409.
19. Yang, D. S., W. C. Hon, …, F. Sicheri. 1998. Identification of the ice-binding surface on a type III antifreeze protein with a ''flatness function'' algorithm. *Biophys. J.* 74:2142–2151.
20. Antson, A. A., D. J. Smith, …, R. E. Hubbard. 2001. Understanding the mechanism of ice binding by type III antifreeze proteins. *J. Mol. Biol.* 305:875–889.
21. Wen, D., and R. A. Laursen. 1992. Structure-function relationships in an antifreeze polypeptide. The role of neutral, polar amino acids. *J. Biol. Chem.* 267:14102–14108.
22. Wen, D., and R. A. Laursen. 1992. A model for binding of an antifreeze polypeptide to ice. *Biophys. J.* 63:1659–1662.
23. DeLuca, C. I., H. Chao, …, P. L. Davies. 1996. Effect of type III antifreeze protein dilution and mutation on the growth inhibition of ice. *Biophys. J.* 71:2346–2355.
24. DeLuca, C. I., R. Comley, and P. L. Davies. 1998. Antifreeze proteins bind independently to ice. *Biophys. J.* 74:1502–1508.
25. Du, N., X. Y. Liu, and C. L. Hew. 2003. Ice nucleation inhibition: mechanism of antifreeze by antifreeze protein. *J. Biol. Chem.* 278:36000–36004.
26. Liu, X. Y., and N. Du. 2004. Zero-sized effect of nano-particles and inverse homogeneous nucleation. Principles of freezing and antifreeze. *J. Biol. Chem.* 279:6124–6131.
27. Du, N., X. Y. Liu, and C. L. Hew. 2006. Aggregation of antifreeze protein and impact on antifreeze activity. *J. Phys. Chem. B.* 110: 20562–20567.
28. Salvay, A. G., J. Santos, and E. I. Howard. 2007. Electro-optical properties characterization of fish type III antifreeze protein. *J. Biol. Phys.* 33:389–397.
29. Ebel, C. 2007. Analytical ultracentrifugation: state of the art and perspectives. *In* Protein Structures: Methods in Protein Structure and Stability Analysis. V. Uversky and E. A. Permyakov, editors. Nova Science Publishers, New York.
30. Svergun, D. I. 1999. Restoring low resolution structure of biological macromolecules from solution scattering using simulated annealing. *Biophys. J.* 76:2879–2886.
31. Demeler, B., and K. E. van Holde. 2004. Sedimentation velocity analysis of highly heterogeneous systems. *Anal. Biochem.* 335:279–288.
32. Schuck, P. 2000. Size-distribution analysis of macromolecules by sedimentation velocity ultracentrifugation and lamm equation modeling. *Biophys. J.* 78:1606–1619.
33. Solovyova, A., P. Schuck, …, C. Ebel. 2001. Non-ideality by sedimentation velocity of halophilic malate dehydrogenase in complex solvents. *Biophys. J.* 81:1868–1880.
34. García De La Torre, J., M. L. Huertas, and B. Carrasco. 2000. Calculation of hydrodynamic properties of globular proteins from their atomic-level structure. *Biophys. J.* 78:719–730.
35. Uversky, V. N. 2002. What does it mean to be natively unfolded? *Eur. J. Biochem.* 269:2–12.
36. Manon, F., and C. Ebel. Analytical ultracentrifugation, a useful tool to probe intrinsically disordered proteins. *In* Instrumental Analysis of Intrinsically Disordered Proteins: Assessing Structure and Conformation. V. N. Uversky and S. Longhi, editors. John Wiley and Sons, Hoboken, NJ. 433–449.
37. Gerard, F. C. A., Ede. A. Ribeiro, Jr., …, M. Jamin. 2007. Unphosphorylated rhabdoviridae phosphoproteins form elongated dimers in solution. *Biochemistry.* 46:10328–10338.
38. Svergun, D. I., S. Richard, …, G. Zaccai. 1998. Protein hydration in solution: experimental observation by x-ray and neutron scattering. *Proc. Natl. Acad. Sci. USA.* 95:2267–2272.
39. Salvay, A. G., and C. Ebel. 2006. Analytical ultracentrifuge for the characterization of detergent in solution. *Prog. Colloid Polym. Sci.* 131: 74–82.
40. Lebaupain, F., A. G. Salvay, …, B. Pucci. 2006. Lactobionamide surfactants with hydrogenated, perfluorinated or hemifluorinated tails: physical-chemical and biochemical characterization. *Langmuir.* 22: 8881–8890.
41. Salvay, A. G., M. Santamaria, …, C. Ebel. 2007. Analytical ultracentrifugation sedimentation velocity for the characterization of detergent-solubilized membrane proteins $Ca^{++}$-ATPase and ExbB. *J. Biol. Phys.* 33:399–419.
42. Hew, C. L., D. Slaughter, …, V. S. Ananthanarayanan. 1984. Antifreeze polypeptides from the Newfoundland ocean pout *Macrozoarces americanus*: presence of multiple and compositionally diverse components. *J. Comp. Physiol. [B].* 155:81–88.
43. Li, X. M., K. Y. Trinh, …, P. L. Davies. 1985. Structure of an antifreeze polypeptide and its precursor from the ocean pout, *Macrozoarces americanus*. *J. Biol. Chem.* 260:12904–12909.

44. Jia, Z., C. I. DeLuca, and P. L. Davies. 1995. Crystallization and preliminary X-ray crystallographic studies on Type III antifreeze protein. *Protein Sci.* 4:1236–1238.

45. Chao, H., P. L. Davies, …, F. D. Sönnichsen. 1993. Use of proline mutants to help solve the NMR solution structure of type III antifreeze protein. *Protein Sci.* 2:1411–1428.

46. Chao, H., F. D. Sönnichsen, …, P. L. Davies. 1994. Structure-function relationship in the globular type III antifreeze protein: identification of a cluster of surface residues required for binding to ice. *Protein Sci.* 3:1760–1769.

47. García-Arribas, O., R. Mateo, …, M. G. Mateu. 2007. Thermodynamic stability of a cold-adapted protein, type III antifreeze protein, and energetic contribution of salt bridges. *Protein Sci.* 16:227–238.

48. Clarkson, J. R., Z. F. Cui, and R. C. Darton. 1999. Protein denaturation in foam. *J. Colloid Interface Sci.* 215:333–338.

49. Leclerc, E., and P. Calmettes. 1997. Structure of $\beta$-casein micelles. *Physica B.* 241:1141–1143.

50. Wustneck, R., J. Krägel, …, D. C. Clark. 1996. The adsorption of surface-active complexes between $\beta$-casein, $\beta$-lactoglobulin and ionic surfactants and their shear rheological behaviour. *Colloid Surf. A Physicochem. Eng. Asp.* 114:255–265.

51. Okubo, T., and K. Kobayashi. 1998. Surface tension of biological polyelectrolyte solutions. *J. Colloid Interface Sci.* 205:433–442.

52. Yampolskaya, G., and D. Platikanov. 2006. Proteins at fluid interfaces: adsorption layers and thin liquid films. *Adv. Colloid Interface Sci.* 128–130:159–183.

53. Zhu, F., J. Kapitan, …, L. D. Barron. 2008. Residual structure in disordered peptides and unfolded proteins from multivariate analysis and ab initio simulation of Raman optical activity data. *Proteins.* 70:823–833.

54. Holland, N. B., Y. Nishimiya, …, F. D. Sönnichsen. 2008. Two domains of RD3 antifreeze protein diffuse independently. *Biochemistry.* 47:5935–5941.

55. Knight, C. A., A. L. DeVries, and L. D. Oolman. 1984. Fish antifreeze protein and the freezing and recrystallization of ice. *Nature.* 308: 295–296.